Modeling of hydrodynamic processes in rotor-pulsation apparatus

Victor Voroshchuk[1], Maria Shynkaryk[1], Pawel Drozdziel[2], Oleh Kravets[1]

1 – Ternopil Ivan Puluj National Technical University, Ternopil, Ukraine
2 – Lublin University of Technology, Lublin, Poland

Keywords:

Rotor
Pulsation
Hydrodynamics
Pressure
Velocity
Simulation
Modelling

Article history:

Received 18.05.2025
Received in revised form 23.10.2025
Accepted 31.12.2025

Corresponding author:

Victor Voroshchuk
E-mail: voroschuk@gmail.com

DOI: 10.24263/2310-1008-2025-13-2-4

Abstract

Introduction. A mathematical model is developed to describe the unsteady flow in the gap between the rotating and stationary elements of a rotor–pulsation apparatus. The model accounts for pressure pulsations and the non-Newtonian behavior of the processed material.

Materials and methods. This study investigates the unsteady flow of a non-Newtonian curd mass in the rotor–stator gap of a rotor–pulsation apparatus using an axisymmetric model in cylindrical coordinates. The flow is governed by the continuity and Navier–Stokes equations, while rheology is described by the Herschel–Bulkley law with a structural parameter accounting for shear-induced breakdown and recovery. Pressure pulsations due to rotor–stator interaction are represented by a harmonic pressure-drop function, and the equations are solved using the finite-volume method in SolidWorks Flow Simulation with local mesh refinement in the rotor–stator gap.

Results and discussion. The numerical results show that, in the rotor speed range of 2000–3500 revolutions per minute, an unsteady flow develops in the rotor–stator gap with a dominant tangential motion. Over a 3.5 s operating cycle, the mean tangential velocity increases with speed, whereas axial transport remains strongly pulsatory. Tangential velocity pulsations are about 3%, axial oscillations reach ~10% of the mean value, and the radial component remains secondary (1–3%). A systematic reduction in throughput is observed with increasing rotor speed: the mean flow rate decreases from 0.00156 to 0.00066 m^3/s, and the processed volume per cycle from 0.00549 to 0.00229 m^3/cycle. The flow rate exhibits periodic oscillations due to rotor–stator interaction; for a twelve-channel rotor, the pulsation frequency increases from approximately 400 to 700 Hz with an amplitude of 5–10% of the mean value. Energy demand increases with speed: the calculated torque rises from 1.13 to 1.98 N·m and power from 223 to 553 W. The nondimensional axial contribution decreases from 0.212 to 0.064, indicating a shift toward a predominantly tangential regime and explaining the reduced throughput. Comparison with experimental data confirms model adequacy, with discrepancies below 10% for power and below 20% for torque.

Conclusions. An integrated unsteady-flow model for the rotor–stator gap was developed. The model captures the twelve-channel pressure pulsations in the frequency range of 400–700 Hz and predicts power consumption with an accuracy better than 10%. The proposed model can be used for hydrodynamic analysis and optimization of rotor-pulsation apparatus operating conditions.

ISSN: 2409-4951 (Online), 2310-1008(Print)

Introduction

Hydrodynamic rotor-pulsation apparatuses (RPAs) are increasingly recognised as effective tools for dispersion, homogenization, emulsification, and the intensification of heat and mass transfer (Samoichuk et al., 2024). Their performance arises from the combined action of turbulent mixing, periodic pressure pulsations, and cavitation within the working chamber, creating a highly dynamic flow environment that is difficult to capture with conventional modelling approaches (Voroshchuk, 2010). Despite notable advances in studying RPA operation, existing mathematical models remain incomplete (Håkansson, 2018; Vashisth et al., 2021). Most assume Newtonian fluid behaviour, which does not represent the complex rheology typical of many food systems (Ahmed et al., 2018; Vashisth et al., 2021). Current modelling efforts can be broadly grouped into three directions (Håkansson, 2018; Vashisth et al., 2021): rheological models describing viscous and structured media (Barnes, 1999); models based on dimensionless criteria and similarity analysis (John et al., 2019); and CFD (Computational Fluid Dynamics) approaches capable of resolving detailed flow fields, pressure distributions, and turbulence characteristics (Minnick et al., 2023; Mortensen et al., 2018).

However, each of the existing modelling strategies captures only a limited part of the hydrodynamic behaviour (Mortensen et al., 2018). Rheological models typically neglect the spatial and temporal structure of the flow, whereas CFD approaches, despite their capabilities, rarely incorporate sufficiently accurate descriptions of non-Newtonian behaviour (Ahmed et al., 2018; Minnick et al., 2023). Methods based on dimensionless groups reveal general trends but are unable to resolve local effects associated with cavitation development or pulsation-induced instabilities (Zheng et al., 2022). These limitations create a clear need for more integrated modelling frameworks that combine rheological and hydrodynamic representations to enhance the predictability of RPA performance under real processing conditions (Samoichuk et al., 2024).

In computational fluid dynamics analyses of rotor-stator systems, the Reynolds-averaged Navier-Stokes formulation is widely used, decomposing velocity and pressure into mean and fluctuating components (Zemanová and Rudolf, 2019). Turbulence closure is most commonly performed using the k-ε and k-ω models, which may differ in accuracy when predicting energy dissipation and the localization of high-gradient zones (Wilcox, 2006) (Table 1). The k-ε model is often selected for its robustness and computational efficiency (Adanta, 2020). The k-ω model, particularly its SST modification (Table 1), provides a more reliable description of near-wall behavior and flow separation (Adanta, 2020). Simulation results supported by experimental observations, including velocity-field validation using particle image velocimetry, have confirmed the applicability of these approaches to rotor-stator mixing flows and to estimating energy dissipation characteristics (Mortensen et al., 2018). These findings also indicate that the geometry of the apparatus can strongly influence mixing efficiency and hydrodynamic behavior (Wang et al., 2023). This effect is consistent with broader analyses of hydrodynamic reactor design and performance trends (Zheng et al., 2022).

Additional insights into flow structure and energy dissipation were presented in (Utomo, 2008), where velocity fields and turbulent energy characteristics were successfully reproduced. For rotor-pulsation apparatuses with axial discharge, the LES (Large Eddy Simulation) approach was applied in (Minnick et al., 2023), yielding detailed predictions of velocity profiles, turbulence statistics, pressure distribution, particle transport, and energy dissipation patterns. Other studies focused on energetic aspects governed by the rotor-stator configuration (Badve et al., 2013) linked the turbulent dissipation rate E_k to the rotor-stator gap, while (Zheng et al., 2022) examined the relationship between power consumption and flow hydrodynamics.

ISSN: 2409-4951 (Online), 2310-1008(Print)

Table 1

Comparison of RANS-based turbulence models

Model type	Advantages	Limitations	Typical applications
k-ε (turbulence model)	Suitable for evaluating energy-related characteristics; simple in formulation; accurate for turbulent flows.	Inaccurate in regions with flow separation; large deviations from experimental data may occur.	Numerical studies of energy dissipation and design improvement (Utomo and Pacek, 2009).
k-ω (turbulence model)	More accurate near-wall predictions; improved evaluation of energy dissipation zones.	Sensitive to boundary and initial conditions; numerical stability may vary.	Analysis of hydrodynamics in rotor-stator gaps (Zemanová & Rudolf, 2019).
SST k-ω (shear-stress transport model)	Combines advantages of k-ε and k-ω; better performance for separated flows and adverse pressure gradients.	Requires extensive input data for proper setup.	CFD model validation (Launder et al, 1974) and model comparison (Mortensen et al., 2018).
RNG k-ε (renormalization-group variant)	Better representation of medium-scale turbulent fluctuations than the standard k-ε model.	Limited applicability for highly turbulent or strongly anisotropic flows.	Studies of rotor-based mixing devices (Vashisth et al., 2021).

As noted earlier, many existing studies (Badve et al., 2013; Ranade, 2022; Wang et al., 2023; Zheng et al., 2022) address Newtonian fluids, underscoring the need for modelling approaches suitable for non-Newtonian media and for capturing the geometric specifics of RPAs. In response to this, the present study develops a hydrodynamic model that incorporates both apparatus design features and experimentally observed rheology. The model is then evaluated through comparison with published data, followed by the formulation of practical recommendations based on the numerical findings.

This study aims to develop an integrated unsteady hydrodynamic model of a rotor-pulsation apparatus that incorporates non-Newtonian rheology and pressure pulsations, and to assess its adequacy by comparing it with published torque and power data.

Materials and methods

Rotor-pulsation apparatus

The study was performed for a rotor-pulsation apparatus (RPA) comprising a rotor and a stator equipped with a system of radial channels, with an annular clearance (gap) formed between the interacting surfaces (Figure 1).

ISSN: 2409-4951 (Online), 2310-1008(Print)

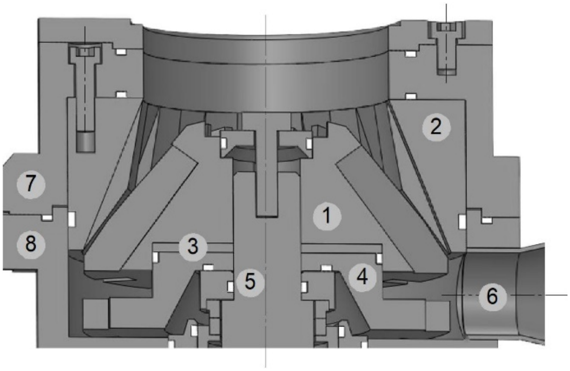

Figure 1. Schematic diagram of the rotor-pulsation apparatus (RPA):
1 – rotor;
2 – stator;
3 – adjustment shim;
4 – pump element;
5 – shaft;
6 – circulation channel;
7 – inlet chamber;
8 – outlet chamber.

The following parameters were used in the calculations: rotor radius R=0.038m, rotor-stator gap δ=1.5mm, number of radial channels z=12. The rotor speed range was 2000–3500 rpm, and the computational cycle duration was 3.5 s. The flow in the rotor-stator clearance was interpreted as the motion of a non-Newtonian medium in an annular gap between two coaxial cylinders. During rotor rotation, the curd mass is sheared in a Couette-type regime; the resulting tangential stresses govern the rotor torque and, consequently, the mechanical power demand (John et al., 2019; Mortensen et al., 2018; Utomo and Pacek, 2009).

Modelling approach and numerical implementation

Hydrodynamic characteristics of the RPA working zone were determined by numerical simulation of unsteady flow in the rotor-stator gap. In addition to circumferential shear, an oscillatory axial component driven by a pulsating pressure drop along the channel axis was considered. The modelling framework was formulated based on the conservation of mass and momentum, while accounting for the non-Newtonian rheological response of the curd mass (Adanta, 2020; Wilcox, 2006; Voroshchuk, 2010; Zemanová and Rudolf, 2019). The non-Newtonian behaviour of the medium was represented using a Herschel-Bulkley-type rheological description with a structural parameter. To represent pulsations, a harmonic time dependence of the imposed pressure drop was prescribed and characterised by its mean value, amplitude, angular frequency, and phase shift. The simulations were carried out using the finite-volume method with semi-implicit time integration in SolidWorks Flow Simulation. Local mesh refinement was applied in the rotor-stator gap.

Processed material (curd mass)

A laboratory-prepared curd mass was used as the working medium. The sample was obtained by thoroughly mixing the components until a homogeneous mass was formed. The formulation (mass fractions) was: curd base – 67.4 wt%, water – 23.0 wt%, and flavor – 9.6 wt%. This curd mass was then used in the simulations and subsequent analysis of hydrodynamic parameters in the RPA working zone.

ISSN: 2409-4951 (Online), 2310-1008(Print)

Results and discussion

Governing equations and mathematical model of the flow

The continuity equation ensuring mass conservation for an axisymmetric flow is written as (Bird et al., 2002; White, 2006; Zemanová and Rudolf, 2019):

$$\frac{1}{r}\frac{\partial\left(rv_r\right)}{\partial r}+\frac{\partial v_z}{\partial z}=0 \ , \tag{1}$$

where v_r is the radial velocity, v_z the axial velocity, and r the radial coordinate (m).

The term $\frac{\partial\left(rv_r\right)}{\partial r}$ represents the radial derivative of mass flux; $\frac{1}{r}\frac{\partial\left(rv_r\right)}{\partial r}$ expresses the relative variation of the radial flux per unit radius; and $\frac{\partial v_z}{\partial z}$ describes the axial change of velocity (1/s). According to this equation, any variation in axial velocity is compensated by the corresponding distribution of radial velocities, ensuring a steady flow in the gap.

To describe the flow dynamics, the Navier-Stokes equations with three velocity components are applied. Each equation governs momentum in the corresponding direction (Bird et al., 2002; White, 2006).

In the radial direction, inertial forces, the centrifugal term u_θ^2/r, the pressure gradient $\partial p/\partial r$, and viscous stresses are taken into account (White, 2006; Zemanová and Rudolf, 2019):

$$\rho\left(\frac{\partial v_r}{\partial t}+v_r\frac{\partial v_r}{\partial r}+v_z\frac{\partial v_r}{\partial z}-\frac{u_\theta^2}{r}\right)=-\frac{\partial p}{\partial r}+\frac{1}{r}\frac{\partial\left(r\tau_{rr}\right)}{\partial r}+\frac{\partial \tau_{rz}}{\partial z}-\frac{\tau_{\theta\theta}}{r} \ , \tag{2}$$

where u_θ is the tangential velocity; ρ the fluid density; p the pressure; τ_{rr} the radial normal stress; $\tau_{\theta\theta}$ the tangential normal stress; and τ_{rz} the shear stress in the r - z plane.

In the tangential direction, momentum transfer from the rotor to the working fluid is dominant (Hop et al., 2023; John et al., 2019; Utomo et al., 2008):

$$\rho\left(\frac{\partial u_\theta}{\partial t}+v_r\frac{\partial u_\theta}{\partial r}+v_z\frac{\partial u_\theta}{\partial z}+\frac{v_r u_\theta}{r}\right)=\frac{1}{r^2}\frac{\partial\left(r^2\tau_{r\theta}\right)}{\partial r}+\frac{\partial \tau_{\theta z}}{\partial z} \ , \tag{3}$$

where $\tau_{r\theta}$ the shear stress in the $r-\theta$ plane; and $\tau_{\theta z}$ the shear stress in the $\theta-z$ plane.

The left-hand side represents inertial transport of tangential momentum, while the right-hand side represents viscous forces. In the axial direction, a pressure drop is needed to drive the product through the channels (Utomo and Pacek, 2009; Utomo et al., 2008):

$$\rho\left(\frac{\partial v_z}{\partial t}+v_r\frac{\partial v_z}{\partial r}+v_z\frac{\partial v_z}{\partial z}\right)=-\frac{\partial p}{\partial z}+\frac{1}{r}\frac{\partial\left(r\tau_{rz}\right)}{\partial r}+\frac{\partial \tau_{zz}}{\partial z} , \tag{4}$$

where τ_{zz} is the axial normal stress.

Since the equations involve stresses, the rheological behaviour of the curd mass must be considered (Barnes, 1999).

ISSN: 2409-4951 (Online), 2310-1008(Print)

The Herschel-Bulkley model (Barnes, 1999; Voroshchuk, 2010) is used

$$\tau = \tau_0 + K\dot{\gamma}^n, \quad \eta_{\text{eff}} = \frac{\tau_0}{\dot{\gamma}} + K\dot{\gamma}^{n-1}, \tag{5}$$

where τ is shear stress (Pa); τ_0 the yield stress (Pa); K the consistency coefficient (Pa·s^n); n the flow index; and $\dot{\gamma} = \sqrt{2D_{ij}D_{ij}}$ the shear-rate intensity (1/s). Here n is the flow index of the Herschel–Bulkley model; the rotor rotational speed is denoted as n_{rot} (rpm) in the Results section.

Unlike Newtonian fluids, curd mass undergoes structural breakdown under shear, reducing effective viscosity, while partial recovery occurs in rest. To account for this behaviour, a structural parameter $\lambda \in [0,1]$ is introduced, modifying τ_0 and K depending on structural integrity. Its evolution follows:

$$\frac{d\lambda}{dt} = \frac{1-\lambda}{T_b} - k_d(\dot{\gamma}, T)\lambda, \tag{6}$$

where T_b is the recovery time and $k_d \propto |\dot{\gamma}|^m$ with temperature correction.

This formulation allows reproduction of both the pulsating nature of flow in the RPA and the gradual decrease in viscosity and shift of mean values of $\dot{\gamma}$ and wall shear stress τ_w from cycle to cycle (Utomo et al., 2008; Samoichuk et al., 2024**.**

As the apparatus operates with periodic pressure fluctuations, the instantaneous pressure drop is described by (Utomo et al., 2008):

$$\Delta p(z,t) = \Delta p_0(z) + A(z)\sin(\omega_p t + \varphi), \tag{7}$$

where $\Delta p_0(z)$ is the mean pressure-drop component, $A(z)$ the pulsation amplitude, ω_p the pulsation angular frequency (rad/s), and φ the phase shift.

Boundary conditions

Rotor (no-slip at rotating wall) (White, 2006; Zemanová and Rudolf, 2019)**:**

$$u_\theta = \omega r,\ v_r = 0,\ v_z = 0. \tag{8}$$

Stator (stationary wall):

$$u_\theta = 0,\ v_r = 0,\ v_z = 0. \tag{9}$$

Outlet (fixed pressure):

$$p = p_{\text{out}}. \tag{10}$$

The influence of axial flow is evaluated using the nondimensional parameter (Hop et al., 2023):

$$\varepsilon = \frac{(v_z)_{A_{\text{out}}}}{U_\theta}, \quad U_\theta = \omega R, \tag{11}$$

where $(v_z)_{A_{\text{out}}}$ is the mean axial velocity at the outlet; ω is the rotor angular velocity (rad/s), $\omega = 2\pi n_{rot}/60$.

The mean axial velocity is defined as:

ISSN: 2409-4951 (Online), 2310-1008(Print)

$$\overline{v_z}(t) = \frac{1}{A_{out}} \int_{A_{out}} v \cdot n_z \, dA, \tag{12}$$

where A_{out} is the outlet area and n_z the axial normal.

Simulations were performed for an RPA with rotor radius R=0.038 m, gap δ=1.5mm, and 12 radial channels. The average channel area was $A_{ch,avr}=7.49 \cdot 10^{-5}$ m², and the total cross-sectional area $A_{tot}=8.988 \cdot 10^{-4}$m². Operational speeds ranged from 2000 to 3000 rpm. A technological cycle duration of 3.5 s was adopted. Computations were axisymmetric with inclusion of tangential velocity.

The continuity equation (1), momentum equations (2) - (5), and rheological model (6) were used. Pulsations were included according to (7), and boundary conditions followed (8) - (10). The finite-volume method with semi-implicit time integration was applied. Mesh refinement was used in the gap to resolve steep velocity gradients. SolidWorks Flow Simulation was employed as the CFD environment (Patankar, 2018; Versteeg and Malalasekera, 2007; John et al., 2019).

The velocity fields $v_r(r,z,t)$, $v_\theta(r,z,t)$, $v_z(r,z,t)$ together with the pressure distribution $p(r,z,t)$ were obtained by solving the governing equations (1)-(4). The effective viscosity η_{eff} was evaluated according to the Herschel-Bulkley relation (6), which incorporates the non-Newtonian rheology of the curd mass.

Based on the computed velocity fields, the instantaneous volumetric flow rate

$$Q(t) = \int_{A_o} utv \cdot n_z dA \tag{13}$$

and the mean axial velocity (12) were determined. The nondimensional parameter ε, characterising the relative contribution of axial transport, was subsequently evaluated. The hydrodynamic torque acting on the rotor was calculated from

$$M(t) = \int_{S_{rot}} r\tau_{r\theta} \, dS \text{, with } \tau_{r\theta} = 2\eta_{eff} D_{r\theta}, \tag{14}$$

where $D_{r\theta}$ is the r−θ component of the strain-rate tensor followed by evaluation of the instantaneous and mean mechanical power (John et al., 2019; Mortensen et al., 2018)**:**

$$N(t) = M(t)\omega \text{, and } \bar{N} = \bar{M}\,\omega . \tag{15}$$

Verification of the numerical solution included comparison with experimental flow-rate measurements, analysis of mesh and time-step sensitivity, assessment of mass conservation between the gap and the outlet section, and evaluation of the overall energy balance (John et al., 2019; Mortensen et al., 2018):

$$\bar{N} \approx \overline{\Delta p\, Q} + \Phi_{\text{losses}} . \tag{16}$$

Φ_{losses} represents additional hydraulic losses, including viscous dissipation and losses associated with vortex structures and secondary flows.

ISSN: 2409-4951 (Online), 2310-1008(Print)

Flow dynamics and cycle-resolved throughput over the operating cycle

Figure 2 presents the theoretical time dependences of the velocity components in the rotor-stator gap during a single 3.5-second operating cycle (results shown within a 0.1-second time window) for rotor rotational speeds n=2000-3500 rpm. The analysed For a rotor components are the tangential velocity $u_\theta(t)$, axial velocity $v_z(t)$, and radial velocity $v_r(t)$, where t denotes time (seconds). The mean tangential velocity u_θ increases with n, whereas its pulsations remain limited (3%). The axial velocity v_z (t) exhibits more pronounced oscillations (10% of the mean value), and its mean value decreases as n increases. The radial velocity v_r remains minor (1–3% of v_z), confirming its secondary contribution to overall transport.

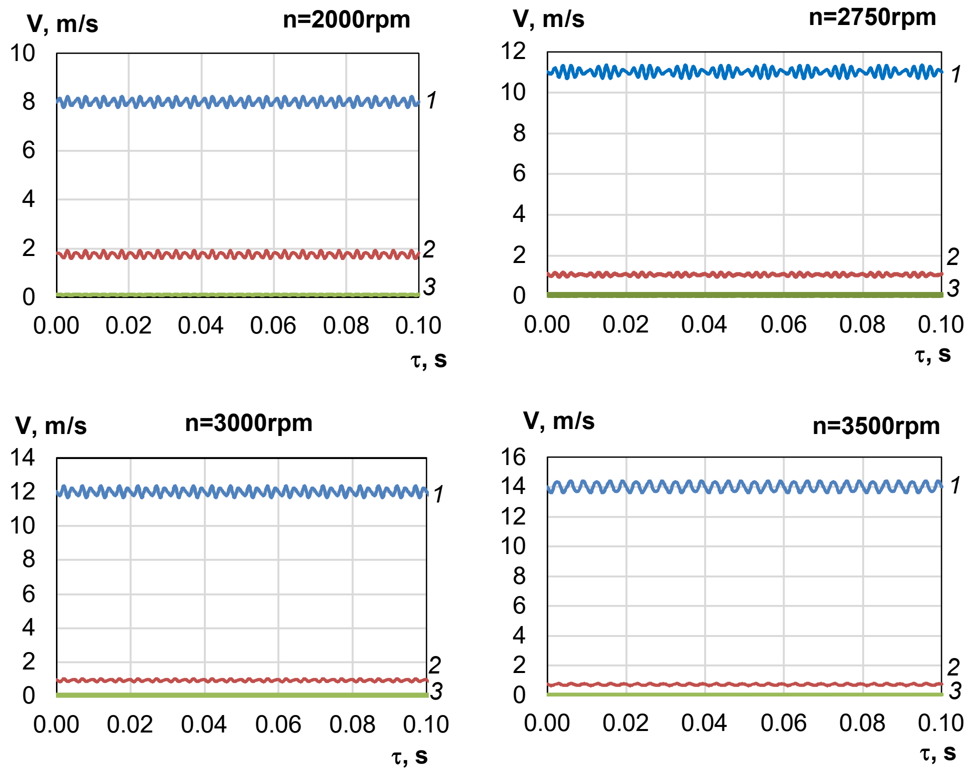

Figure 2. Theoretical time dependences of the velocity components within a single 3.5-second operating cycle (results shown within a 0.1-second time window);
1 – tangential velocity $u_\theta(t)$; 2 – axial velocity $v_z(t)$; 3 – radial velocity $v_r(t)$.

From the graphical dependencies (Figure 2), it is observed that the mean tangential velocity u_θ increases proportionally with the rotational speed n (2000–3500 rpm). The pulsations of u_θ are about 3 percent, which is consistent with the 2-5 percent reported in (Utomo et al., 2008; Mortensen et al., 2018). The axial velocity $v_z\left(t\right)$ exhibits oscillations of

ISSN: 2409-4951 (Online), 2310-1008(Print)

approximately 10 percent of its mean value, which corresponds to the 8-12 percent range noted in (Mortensen et al., 2018). Although the mean value of v_z decreases with increasing n, the pulsatory behaviour remains. The radial velocity v_r accounts for only 1–3 percent of v_z, confirming its minor contribution, as also indicated in (Samoichuk et al., 2024) and (Launder et al., 2010; Utomo and Pacek, 2009).

Using the calculated velocity functions $u_\theta(t)$, $v_z(t)$, and $v_r(t)$, the instantaneous flow rate was determined as:

$$Q(t) = v_z(t) \cdot A_{\text{tot}}, \tag{16}$$

where A_{tot} is the total cross-sectional area.

Integration of $Q(t)$ over one 3.5-second operating cycle yields the total processed volume per cycle V_{tot}:

$$V_{\text{tot}} = \int_0^T Q(t)\,dt,$$

where T = 3.5 seconds is the cycle duration.

Figure 3 presents the variations of the instantaneous flow rate Q(t) and the accumulated volume $V_{tot}(t)$ over a single operating cycle for rotor rotational speeds n=2000–3500 rpm.

As shown in Figure 3, the instantaneous flow rate $Q(t)$ exhibits a clearly pronounced periodic pattern. The oscillations are quasi-regular and reflect the periodic interaction between the rotor channels and the stator (blade-passing effect), which modulates the axial velocity component and, consequently, the instantaneous throughput. The relative amplitude of the flow-rate oscillations is about 5–10%, which is consistent with LES/CFD studies (Mortensen et al., 2018; Utomo et al., 2008).

The accumulated volume $V_{tot}(t)$ shows an almost linear increase over the cycle, confirming that the net transport remains stable despite the pulsations of Q(t). Importantly, the slope of $V_{tot}(t)$ (i.e., the cycle-averaged throughput) decreases as n increases, indicating a weakening of axial transport at higher rotor speeds. This behaviour is consistent with Taylor-Couette type flows, where exceeding a critical rotational speed promotes stable vortex structures that reduce axial transport (Hop et al., 2023; Launder et al., 2010).

Experimental validation of hydraulic and energy characteristics of the rotor-stator system

To assess the adequacy of the proposed model, the predicted mean characteristics were compared with experimental data (Voroshchuk, 2010), including the mean liquid flow rate *Q*, torque M, and power N as functions of the rotor rotational speed *n*. As shown in Figure 4, the mean liquid flow rate decreases with increasing rotor speed. The predicted values agree well with the experimental dataset, supporting the adequacy of the model. The reduction in Q with increasing n is explained by the rise in hydraulic resistance and the development of vortex structures within the rotor-stator gap, which decreases the contribution of the axial flow component to transport (Zheng et al., 2022).

ISSN: 2409-4951 (Online), 2310-1008(Print)

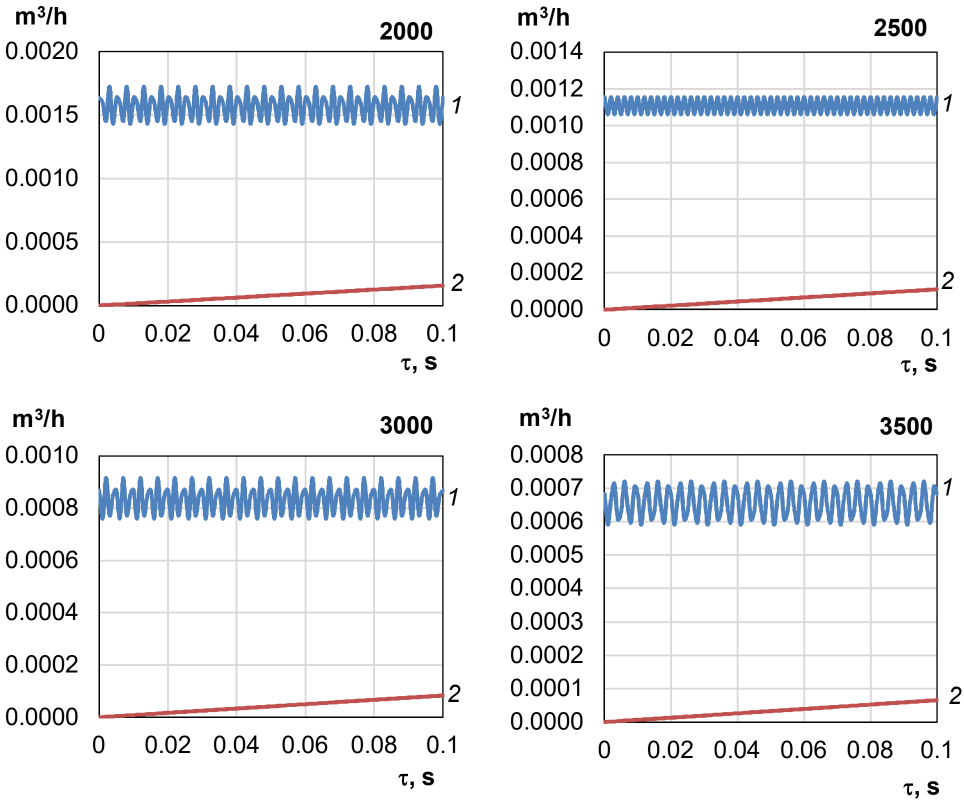

Figure 3. Instantaneous flow rate $Q(t)$ and accumulated (processed) volume $V_{tot}(t)$ over a single 3.5-second operating cycle: 1 – $Q(t)$; 2 – $V_{tot}(t)$

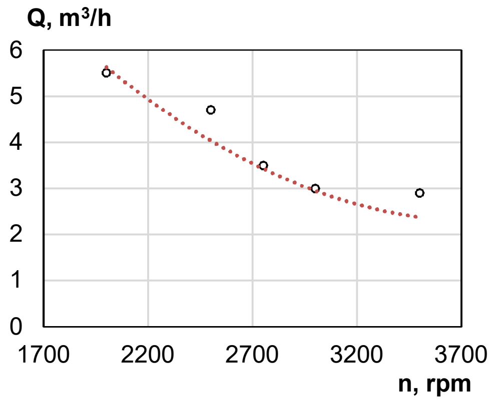

Figure 4. Mean liquid flow rate Q as a function of rotor rotational speed n:
—— calculated (theoretical) values;
◦ experimental values
(Voroshchuk, 2010).

ISSN: 2409-4951 (Online), 2310-1008(Print)

The results presented in Figure 4 demonstrate a decrease in the mean liquid flow rate Q with increasing rotor rotational speed n. The predicted mean values agree well with the experimental data (Voroshchuk, 2010), which confirms the adequacy of the model. The reduction in the mean liquid flow rate Q with increasing rotor rotational speed n is explained by the rise in hydraulic resistance, the formation of vortex structures within the rotor-stator gap, and, consequently, the decrease in the contribution of the axial flow component to overall transport. This observation is consistent with the findings of Zheng et al. (2022).

CFD studies of rotor-cavitation devices also indicate that, as the rotor rotational speed increases, the tangential flow components increasingly dominate the hydrodynamics, whereas the contribution of the axial component diminishes (Ranade, 2022). Similar hydrodynamic behaviour is observed in classical Taylor-Couette-type flows, where exceeding the critical rotational speed leads to the formation of stable vortex structures that weaken the axial flow and the corresponding transport (Hop et al., 2023).

The results for the torque M and power N reflect the increase in energy consumption associated with overcoming viscous resistance and generating circulating flow structures. It should be noted that the axial-flow contribution coefficient ε\varepsilonε decreases from 0.21 to 0.064, which is attributed to the transition in the flow structure-from a combined pattern (axial and tangential components) at low rotor rotational speeds to a predominantly tangential pattern at higher nnn.

Figures 5 and 6 present graphical comparisons between the values calculated using the proposed model and the corresponding experimental data (Voroshchuk, 2010).

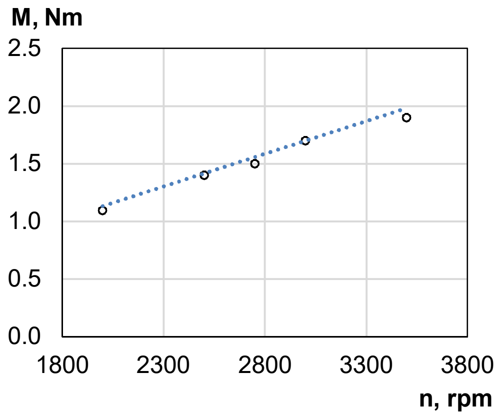

Figure 5. Dependence of torque M on rotor rotational speed n:
—— calculated (theoretical) values;
◦ experimental values
(Voroshchuk, 2010)

The torque M increases with rotor rotational speed n, consistent with intensified shear in the rotor-stator gap. The model-predicted (calculated) mean torque agrees well with the experimental data, and the calculated (n) trend is close to linear, indicating an approximately proportional relationship between the tangential flow velocity and viscous resistance. The deviation between experiment and model does not exceed 5-7% at n=2000-2500 rpm and remains below 20% at n=3000-3500 rpm. The remaining discrepancy is attributed to additional losses related to vortex structures and secondary flows that are difficult to capture analytically; similar effects at higher n have been reported in Wang et al. (2023), Zheng et al. (2022), and Ranade (2022).

ISSN: 2409-4951 (Online), 2310-1008(Print)

Figure 6 presents a comparison of the calculated and experimental power values.

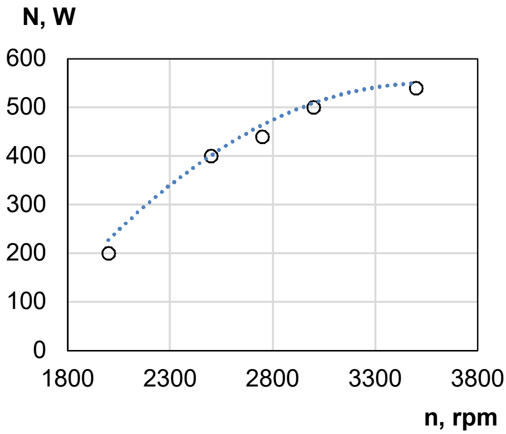

Figure 6. Comparison of calculated and experimental power N as function of rotor rotational speed n:
—— calculated (theoretical) values;
◦ experimental values
(Voroshchuk, 2010).

The predicted mean power values show good agreement with experiments, indicating that the adopted model adequately reproduces the energy consumption of the apparatus. The relationship $N = f(n)$ exhibits an almost linear trend over the investigated range, and the discrepancy between theoretical and experimental data does not exceed 10%. This deviation may be attributed to additional energy losses not fully captured by the model (Wang et al., 2023; Utomo et al., 2008; Zheng et al., 2022).

Conclusions

Existing approaches to describing rotor–pulsation devices are not fully universal: rheological models capture material behavior but ignore flow structure, while CFD methods reconstruct velocity and pressure fields but are mainly for Newtonian fluids. To address this, an integrated approach was developed, incorporating the non-Newtonian nature of curd mass via a structural parameter for shear-induced breakdown and recovery, and a harmonic function to represent flow oscillations. It was found that increasing rotor speed decreases mean flow rate and processed volume, while tangential flow dominates the hydrodynamic pattern. Flow pulsations, determined by rotor channel number and speed, reach 5–10% of the mean value, consistent with prior studies. Comparison with experimental data shows good agreement for performance and energy characteristics, confirming model adequacy. The results suggest operating at lower speeds to maximize processed volume and at higher speeds to intensify shear, dispersion, or homogenization. Further work could extend design parameters, refine rheological models, and apply 3D CFD (LES/URANS) to study secondary flows and vortex structures.

References

Adanta D., Fattah I.M.R., Muhammad N.M. (2020), Comparison of standard k-ε and SST k-ω turbulence model for breastshot waterwheel simulation, *Journal of Mechanical Science and Engineering*, 7(2), pp. 39–44, https://doi.org/10.36706/jmse.v7i2.44

Ahmed U., Michael V., Hou R., Mothersdale T., Prosser R., Kowalski A., Martin P. (2018), An energy transport based evolving rheology in high-shear rotor–stator mixers, *Chemical Engineering Research and Design*, 133, pp. 398–406, https://doi.org/10.1016/j.cherd.2018.02.019

Badve M., Gogate P.R., Pandit A.B., Csoka L. (2013), Hydrodynamic cavitation as a novel approach for wastewater treatment in wood finishing industry, *Separation and Purification Technology*, 106, pp. 15–21, https://doi.org/10.1016/j.seppur.2012.12.029

Barnes H.A. (1999), The yield stress – a review or 'panta rei' – everything flows?, *Journal of Non-Newtonian Fluid Mechanics*, 81(1–2), pp. 133–178, https://doi.org/10.1016/S0377-0257(98)00094-9

Bird R.B., Stewart W.E., Lightfoot E.N. (2002), *Transport Phenomena*, 2nd ed., John Wiley & Sons, New York.

Hakansson A. (2018), Rotor-stator mixers: from batch to continuous mode of operation – a review, *Processes*, 6(4), 32, https://doi.org/10.3390/pr6040032

Hop C.J.W., Jansen R., Besten M., Chaudhuri A., Baltussen M.W., van der Schaaf J. (2023), Hydrodynamics of a rotor–stator spinning disk reactor, investigations by large-eddy simulation, *Physics of Fluids*, 35(3), 035105, https://doi.org/10.1063/5.0137405

John T.P., Panesar J.S., Kowalski A., Rodgers T.L., Fonte C.P. (2019), Linking power and flow in rotor-stator mixers, *Chemical Engineering Science*, 207, pp. 504–515, https://doi.org/10.1016/j.ces.2019.06.039

Launder B.E., Poncet S., Serre E. (2010), Laminar, transitional, and turbulent flows in rotor-stator cavities, *Annual Review of Fluid Mechanics*, 42, pp. 229–248, https://doi.org/10.1146/annurev-fluid-121108-145514

Launder B.E., Spalding D.B. (1974), The numerical computation of turbulent flows, *Computer Methods in Applied Mechanics and Engineering*, 3(2), pp. 269–289, https://doi.org/10.1016/0045-7825(74)90029-2

Minnick B.A., Janz E.E., Calabrese R.V. (2023), CFD simulation of an axial discharge rotor-stator mixer, LES versus RANS predictions, *Chemical Engineering Research and Design*, 198, pp. 413–430, https://doi.org/10.1016/j.cherd.2023.08.047

Mortensen H.H., Arlov D., Innings F., Hakansson A. (2018), A validation of commonly used CFD methods applied to rotor stator mixers using PIV measurements of fluid velocity and turbulence, *Chemical Engineering Science*, 177, pp. 340–353, https://doi.org/10.1016/j.ces.2017.11.037

Patankar S.V. (2018), *Numerical Heat Transfer and Fluid Flow*, CRC Press, Boca Raton, https://doi.org/10.1201/9781482234213

Ranade V.V. (2022), Modeling of hydrodynamic cavitation reactors, reflections on present status and path forward, *ACS Engineering Au*, 2(6), pp. 461–476, https://doi.org/10.1021/acsengineeringau.2c00025

Samoichuk K., Yalpachyk V., Kholobtseva I., Dmytrevskyi D., Chervonyi V. (2024), Design improvement of the rotary-pulsation device by resonance phenomena, In: *Advances in Design, Simulation and Manufacturing VII, Lecture Notes in Mechanical Engineering*, Springer Nature Switzerland, Cham, pp. 74–83, https://doi.org/10.1007/978-3-031-63720-9_7

Utomo A., Baker M., Pacek A.W. (2009), The effect of stator geometry on the flow pattern and energy dissipation rate in a rotor–stator mixer, *Chemical Engineering Research and Design*, 87(4), pp. 533–542, https://doi.org/10.1016/j.cherd.2008.12.011

ISSN: 2409-4951 (Online), 2310-1008(Print)

Utomo A.T., Baker M., Pacek A.W. (2008), Flow pattern, periodicity and energy dissipation in a batch rotor–stator mixer, *Chemical Engineering Research and Design*, 86(12), pp. 1397–1409, https://doi.org/10.1016/j.cherd.2008.07.012

Versteeg H.K., Malalasekera W. (2007), *An Introduction to Computational Fluid Dynamics, The Finite Volume Method,* 2nd ed., Pearson Education, Harlow.

Vashisth V., Nigam K.D.P., Kumar V. (2021), Design and development of high shear mixers, fundamentals, applications and recent progress, *Chemical Engineering Science*, 232, 116296, https://doi.org/10.1016/j.ces.2020.116296

Voroshchuk V.Ya. (2010), *Hidrodynamichni protsesy obrobky syrkovykh mas v rotorno-vykhorovomu emulsori*, *PhD thesis*, Kyiv.

Wang Y., Li M., Liu H.L., Chen J., Lv L.L., Wang X.L., Zhang G.X. (2023), Optimized geometric structure of a rotational hydrodynamic cavitation reactor, *Journal of Applied Fluid Mechanics*, 16(6), pp. 1218–1231, https://doi.org/10.47176/jafm.16.06.1495

White F.M. (2006), *Viscous Fluid Flow*, 3rd ed., McGraw-Hill, New York.

Wilcox D.C. (2006*), Turbulence Modeling for CFD, 3rd ed.,* DCW Industries, La Canada, CA.

Zemanova L., Rudolf P. (2019), Turbulence models for simulation of the flow in a rotor-stator cavity, *EPJ Web of Conferences*, 213, 02104, https://doi.org/10.1051/epjconf/201921302104

Zheng H., Zheng Y., Zhu J. (2022), Recent developments in hydrodynamic cavitation reactors, cavitation mechanism, reactor design, and applications, *Engineering*, 19, pp. 180–198, https://doi.org/10.1016/j.eng.2022.04.027

Author identifiers ORCID

Victor Voroshchuk	0000-0002-8943-1493
Maria Shynkaryk	0000-0003-3489-9803
Pawel Drozdziel	0000-0003-2187-1633
Oleh Kravets	0000-0002-3309-9962

Cite:

Ukr J Food Sci Style

Voroshchuk V., Shynkaryk P., Drozdziel P., Kravets O. (2025), Modeling of hydrodynamic processes in rotor-pulsation apparatus, *Ukrainian Journal of Food Science*, 13(2), pp. 136–149, https://doi.org/10.24263/2310-1008-2025-13-2-4

APA Style

Voroshchuk, V., Shynkaryk, P., Drozdziel, P., & Kravets, O.(2025). Modeling of hydrodynamic processes in rotor-pulsation apparatus. *Ukrainian Journal of Food Science, 13*(2), 136–149. https://doi.org/10.24263/2310-1008-2025-13-2-4